Isothermal equation of state for gold with a He-pressure medium

K. Takemura[1,*] and A. Dewaele[2]
[1]*National Institute for Materials Science (NIMS), Tsukuba, Ibaraki 305-0044, Japan*
[2]*Département de Physique Théorique et Appliquée, CEA, Bruyères-le-Châtel, F-91297 Arpajon Cedex, France*
(Received 2 June 2008; revised manuscript received 1 September 2008; published 29 September 2008)

The isothermal equation of state (EOS) for gold has been determined by powder x-ray diffraction experiments up to 123 GPa at room temperature. We have performed experiments independently in two institutions to check the consistency of the results. A He-pressure medium was used to minimize the effect of uniaxial stress on the sample volume and ruby pressures. The stress state in the He-pressure medium gradually becomes nonhydrostatic above about 30 GPa, with the magnitude of the uniaxial stress largely depending on experiments. Since the measured lattice spacings deviate under different stress states, it is a likely cause of the disagreement of the EOS parameters found in the literature. The lattice spacing d_{111} for the 111 reflection is least affected by the uniaxial stress in the case of gold. Hence we have calculated the sample volume from d_{111} and fitted the obtained pressure-volume data to the Vinet form of EOS. The bulk modulus B_0 at atmospheric pressure was fixed to 167 GPa, a value well established by ultrasonic measurements. The fit gives the pressure derivative of the bulk modulus at atmospheric pressure as $B_0'=5.5(1)$ for the current ruby pressure scale after Zha *et al.* [Proc. Natl. Acad. Sci. U.S.A. **97**, 13494 (2000)]. Alternatively, if we use a different calibration of this standard [Phys. Rev. B **75**, 024115 (2007)], we obtain $B_0'=5.9(1)$, which is in excellent agreement with the ultrasonic measurements and first-principles calculations. Discussions are given to the use of gold as a pressure standard and the hydrostaticity of the He-pressure medium.

DOI: 10.1103/PhysRevB.78.104119 PACS number(s): 64.30.Ef, 62.20.D−, 62.50.−p, 61.05.cp

I. INTRODUCTION

Gold has a number of ideal properties as a pressure standard, such as moderate compressibility, chemical inertness, and large x-ray scattering power. Many high-pressure experiments have been done to establish its equation of state (EOS), yet there is still disagreement in the EOS parameters. Table I summarizes the bulk modulus B_0 and its pressure derivative B_0' of gold at atmospheric pressure found in the literature. Although the value of B_0 is well established ($B_0 \sim 167$ GPa), there is large disagreement in the pressure derivative B_0'. The difference in B_0' is a serious problem when one determines pressure from the EOS of Au as the difference in pressure divergently increases with pressure. Recent debates on the origin of the seismic discontinuity in the earth's lower mantle critically depend on the gold pressure scale.[19–21]

There are several experimental factors, which cause the disagreement of the EOS parameters: experimental methods, pressure scales, EOS formula, pressure-transmitting medium, and so on. Even if the experimental method is the same, systematic differences are noticed, for example, in the powder x-ray diffraction data with the diamond-anvil cell (DAC).[13,22] The x-ray diffraction data by Takemura[22] were analyzed by Shim *et al.*,[12] who obtained a value of $B_0'=5.01$. Dewaele *et al.*[13] also took the powder x-ray diffraction data of gold under high pressure and obtained a value of $B_0'=5.71$. The data by Takemura are more compressible than the data by Dewaele *et al.*, where the pressure difference reaches 5 GPa at 70 GPa. Since the two measurements used the same experimental method and techniques (powder x-ray diffraction in an angle-dispersive mode, DAC with a He-pressure medium, and ruby as a pressure calibrant), such a large difference was difficult to understand unless some systematic errors existed in either one or both experiments. In order to clarify the origin of the disagreement, we have reanalyzed the respective data and found that the stress states in the two measurements were completely different, which produced systematic deviations in the sample volume in opposite directions.[15,23]

In the present paper we report the results of our diffraction experiments carried out at two institutions, which were aimed at better constraining the EOS parameters of gold. We have confirmed our previous observation[15,23] that the stress states of the gold sample compressed in solid He differ by experimental runs, which becomes evident above about 30 GPa. We have thoroughly analyzed the uniaxial stress components in our experimental data including previous ones and obtained most probable values of the EOS parameters of gold.

II. EVALUATION OF THE STRESS STATES

In order to establish the EOS, the sample pressure and volume should be known with high precision and accuracy. It is desirable to achieve purely hydrostatic conditions in the sample chamber, but even helium becomes solid above about 12 GPa at room temperature.[24] The stress condition above that pressure can be nonhydrostatic, and we have to carefully evaluate the stress states in each experiment. Since we determine pressure from the ruby luminescence spectra and the sample volume from powder x-ray diffraction patterns, we summarize the effects of stress in the two cases.

A. Ruby luminescence spectra

Stress conditions are examined in ruby luminescence spectra by checking the following three quantities: (1) the

TABLE I. Bulk modulus B_0, and its pressure derivative B_0', of gold at atmospheric pressure. Adiabatic bulk moduli and its pressure derivatives are converted to isothermal values in the case of ultrasonic measurements (Ref. 1). P_{max} is the maximum pressure investigated. Ultrasonic (US), shock wave (SW), and x-ray diffraction (XRD).

B_0 (GPa)	B_0'	P_{max} (GPa)	Method	Pressure scale	Ref.
166.1	6.49	1.0	US		Daniels and Smith (Ref. 2)
167.1	5.26	0.006	US		Hiki and Granato (Ref. 3)
166.7	6.21	1.0	US		Golding *et al.* (Ref. 4)
166.8	6.26	0.25	US		Biswas *et al.* (Ref. 5)
171	5.0	83	SW		Jamieson *et al.* (Ref. 6)
167	5.5	70	XRD	Ruby (Ref. 7)	Heinz and Jeanloz (Ref. 8)
166.3	6.24	145	XRD	Pt (Ref. 9)	Akahama *et al.* (Ref. 10)
167	5.01	75	XRD	Ruby (Ref. 11)	Shim *et al.* (Ref. 12)
167	5.71	90	XRD	Ruby (Ref. 11)	Dewaele *et al.* (Ref. 13)
167	6.00	93.6	XRD	Ruby (Ref. 13)	Dewaele *et al.* (Ref. 13)
167	5.46	90	XRD	Ruby (Ref. 14)	Takemura (Ref. 15)
166.7	6.12	~230	Theory		Tsuchiya (Ref. 16)
165	5.9	~250	Theory		Souvatzis *et al.* (Ref. 17)
166.70	6.00	~250	Semiempirical		Dorogokupets and Oganov (Ref. 18)
167	5.5	123	XRD	Ruby (Ref. 14)	Present work
167	5.9	131	XRD	Ruby (Ref. 18)	Present work

pressure difference among ruby grains spread in the sample chamber (pressure distribution), (2) the peak width of the ruby R_1 luminescence line, and (3) the separation of the R_1 and R_2 luminescence lines. The pressure difference (1) appears in the case of a hard-pressure medium, in which large nonhydrostatic stress can be sustained.[25] In the case of a He-pressure medium, the pressure difference in the sample chamber has been reported to be as small as 0.6% at 60 GPa,[26] and hence this method is not very effective to detect small stresses. The width of the R_1 luminescence line (2) usually broadens if the ruby grain is subjected to nonhydrostatic stress. If the stress is purely uniaxial, however, no peak broadening is observed in the R_1 and R_2 lines.[27] Hence the sharp luminescence peaks do not necessarily indicate good quasihydrostatic conditions.[28] On the other hand, the R_1-R_2 separation (3) is quite sensitive to uniaxial stress, although the separation depends on the stress direction relative to the crystallographic orientation of ruby.[27] We therefore check both the R_1 peak width and the R_1-R_2 separation in the present work. We have to bear in mind that the stress detected by ruby may not be identical to the stress in the sample, as the stress state is not homogeneous under nonhydrostatic stress.

B. Powder x-ray diffraction patterns

For the cubic system, the lattice parameter (and the volume) is directly obtained from the measured d spacings. If the stress is hydrostatic, the lattice parameter is independent of hkl indices. If the stress is nonhydrostatic, the measured lattice parameter systematically deviates from the hydrostatic value depending on the hkl indices.[29,30]

The stress state in the sample chamber of a DAC with a solid-pressure medium is often approximated to be uniaxial, where the stress along the load direction (axial direction) is larger than that along the radial direction. The uniaxial stress component t is defined as $t=\sigma_3-\sigma_1$, where σ_3 and σ_1 are the stress components in the axial and radial directions, respectively. After the notation in Ref. 30, the measured lattice parameter $a_m(hkl)$ is related to the uniaxial stress component, the orientation of the diffracting plane, and the elastic modulus of the sample and is expressed as

$$a_m(hkl) = M_0 + M_1[3(1 - 3\sin^2\theta)\Gamma(hkl)], \quad (1)$$

where

$$M_0 = a_p\{1 + (\alpha t/3)(1 - 3\sin^2\theta)[S_{11} - S_{12} - (1 - \alpha^{-1}) \times (2G_V)^{-1}]\}, \quad (2)$$

$$M_1 = -a_p\alpha t S/3, \quad (3)$$

$$\Gamma(hkl) = (h^2k^2 + k^2l^2 + l^2h^2)/(h^2 + k^2 + l^2)^2, \quad (4)$$

$$S = S_{11} - S_{12} - S_{44}/2. \quad (5)$$

Here a_p is the lattice parameter under hydrostatic pressure, S_{ij} is the single-crystal elastic compliance, and G_V is the shear modulus of the polycrystalline aggregate under the assumption of strain continuity across the grain boundaries. The parameter α decides the actual stress of the sample that is assumed to lie between the two extreme conditions of stress and strain continuity and takes a value between 0.5 and 1. If we assume that $M_0 \sim a_p$ in Eq. (2) and replace a_p with M_0 in Eq. (3), then we obtain the following relation:

TABLE II. Experimental conditions for high-pressure powder x-ray diffraction measurements on gold. Runs 1–4 are our previous experiments and runs 5–7 are present ones. Runs 1, 5, and 6 were performed at PF and runs 2, 3, 4, and 7 at ESRF.

			Sample		X ray		
Run	Diamond Culet (μm)	P_{max} (GPa)	Form	Size (μm^3)	Wavelength (Å)	Size (μm^2)	Ref.
1	300	75.3	Foil	$40\times40\times1$	0.6198	$\sim40\times40$	Ref. 22
2	400	30.1	Powder	$3\times3\times3$	0.3738	4×6	Ref. 13
3	100/300	90	Powder	$3\times3\times3$	0.3738	4×6	Ref. 13
4	150/350	85.6	Powder	$3\times3\times3$	0.3738	4×6	Ref. 13
5	300	60.8	Foil	$30\times30\times1$	0.4260	$\sim30\times30$	Present work
6	300	63.2	Powder	$\sim30\times30\times30$	0.4260	$\sim30\times30$	Present work
7	100/300	122.5	Powder	$3\times3\times3$	0.3738	2×3	Present work

$$t \sim -3M_1/(\alpha M_0 S). \quad (6)$$

It follows that t is obtained from the slope M_1 and intercept M_0 of a plot $a_m(hkl)$ versus $3(1-3\sin^2\theta)\ \Gamma(hkl)$, termed the Γ plot together with α and S.

III. EXPERIMENTAL METHODS

High-pressure powder x-ray diffraction experiments have been done with DACs with a He-pressure medium at room temperature. In order to check the consistency of the experimental results, independent experiments were carried out at the Photon Factory (PF) and the European Synchrotron Radiation Facility (ESRF). We used nearly the same experimental techniques: DAC with a He-pressure medium, ruby pressure calibrant, powder x-ray diffraction in an angle-dispersive mode, and an imaging plate detector. We use the ruby scale proposed for a He medium with the following formula:

$$P = (A/B)[(\lambda/\lambda_0)^B - 1], \quad (7)$$

where λ and λ_0 are the wavelength of the ruby R_1 luminescence line at high and atmospheric pressures, respectively, $A=1904$ GPa, and $B=7.715$.[14] It should be noted that this scale gives about 0.1% higher pressure compared with the ruby scale most commonly used ($A=1904$ GPa and $B=7.665$).[11] In recent years several investigations claimed that these ruby scales underestimate the pressure by about 5% in the 100 GPa pressure range. This was first noticed by Aleksandrov *et al.* in the measurements of Raman-scattering frequency and EOS of diamond under high pressure.[31] Later on, similar claims have been done based on the comparison of the EOSs of metals studied by shock compression experiments with DAC-EOS data.[13,18,32,33] We therefore compare the pressure based on a different ruby scale with the formula

$$P' = C(\lambda/\lambda_0 - 1)[1 + D(\lambda/\lambda_0 - 1)], \quad (8)$$

where $C=1884$ GPa and $D=5.5$.[18] This scale gives pressure about 6% higher than that determined by Eq. (7) at 100 GPa. We remark that the scale given by Eq. (8) agrees well with another scale, which has the same formula as Eq. (7) with $A=1904$ GPa and $B=9.5$.[13] In the present paper, we basically use the pressure P based on Eq. (7) and discuss the difference of the EOS parameters if we use the pressure values P' based on Eq. (8).

Table II summarizes the experimental conditions for all our experimental data on gold, including previous experimental runs 1–4. The reader is referred to the respective literature for the details of these runs. Experimental details of new runs 5–7 are described below.

A. Runs 5 and 6

Two forms of gold, foil and powder, were used in runs 5 and 6, respectively. The gold foil was 1 μm thick with stated purity of 99.95% purchased from Nilaco Co. Ltd. The gold powder had an average particle size of 0.7 μm with well-defined spherical shape, which was purchased from Ishifuku Metal Co. Ltd. The stated purity was better than 99.9%. The measured lattice parameters of the gold samples at atmospheric pressure and at 25 °C were 4.0788(4) Å for the foil and 4.0787(3) Å for the powder. These values are in excellent agreement with the literature value of 4.0786(2) Å.[34] We use the literature value as a reference in later analysis.

A small piece of the gold foil or a small aggregate of the gold powder was put in the hole of a rhenium gasket. Notice that the aggregate consisted of fine powders of gold, in which gold grains were in loose contact with each other. Tiny ruby spheres (3–4 μm) were put on the surface of one of the diamond anvils. Special care was taken to locate the gold sample at the center of the gasket hole so that the sample was isolated from the gasket wall even if the gasket hole shrank at high pressures. The ruby spheres were placed close to the gold sample. The He-pressure medium was loaded to the DAC at gas pressure of 180 MPa at room temperature.[35] Figure 1 shows the sample and ruby spheres in the gasket hole at the highest pressure in run 5. We relaxed the pressure in the DAC for at least 2 h after each pressure change and thereafter took x-ray diffraction patterns. The pressure changes before and after the x-ray measurement was less than 0.1 GPa at 50 GPa.

The high-pressure powder x-ray diffraction experiments were done on the multipole wiggler beamline BL-13A at PF.

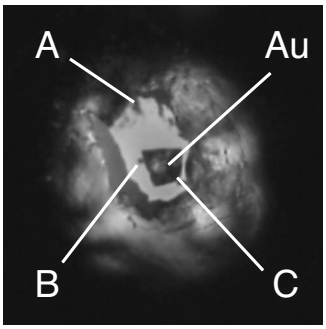

FIG. 1. Sample assembly for the experimental run 5 at 61 GPa. Pressure is based on the ruby scale by Zha *et al.* (Ref. 14) unless otherwise indicated. The microphotograph shows the gold sample (foil with $\sim 30 \times 30 \times 1$ μm^3) and three ruby spheres A, B, and C compressed together with a He-pressure medium in the gasket hole. The edge of the anvil surface is not visible because of the deformation (cupping) of the diamond anvil under high pressure.

The white x rays were monochromatized to a wavelength of 0.4260 Å. Diffracted x rays were recorded on an imaging plate detector (Rigaku R-AXIS). Typical exposure time was 5 min. The powder data were analyzed with the pattern integration software pip.[36]

B. Run 7

A single grain of gold powder (Alfa Aesar product with 99.96% purity) was loaded in helium along with a small ruby sphere (less than 4 μm in diameter) in the hole of a rhenium gasket in a membrane anvil cell. The distance between the sample and the ruby pressure sensor was a few microns. Helium was loaded at ambient temperature under a pressure of approximately 200 MPa. The x-ray diffraction measurements were performed on the ID27 beamline of ESRF in the monochromatic mode. The diffraction parameters or geometry were determined using an iodine absorber (absorption edge corresponding to a wavelength of 0.3738 Å) and a reference silicon sample. The pressure on the sample (increase, stabilization) was monitored through the membrane pressure. For each step, the pressure was stabilized during approximately 1 h (less at very high pressure) and the ruby luminescence signal was recorded immediately after the 20 s x-ray exposure. The run was stopped around 123 GPa when the bridging of the ruby sphere between the diamond anvils was detected. The d spacings for gold have been individually fitted after circular integration of the bidimensional (MAR-CCD detector) signal.

IV. RESULTS

Figure 2 shows the x-ray diffraction patterns and the raw diffraction images of the gold foil at low and high pressures in run 5. The raw image showed strong texture, which was already present in the starting sample. The diffraction intensities are affected by the texture, and some diffraction peaks (e.g., 220 reflection) are even absent at high pressure. This is a demerit to use foil as a pressure marker. Figures 3 and 4 show the diffraction patterns of the powder samples (runs 6 and 7) and raw diffraction images. The raw image of the powder sample shows smooth diffraction rings with uniform diffraction intensities. In run 7, a few single-crystal diffraction spots were observed but have been removed for the data analysis. The powder sample seems to be a better choice for the pressure marker, but if we compare the diffraction patterns in Figs. 2(b) and 3(b), the peak width of the powder sample is much wider than those of the foil. This may indicate the presence of microscopic stress between powder grains. It can be seen in Fig. 4 that the diffraction peaks are wider for run 7, which can be due to instrumental factors, grain size of the powder sample, or microscopic stress.

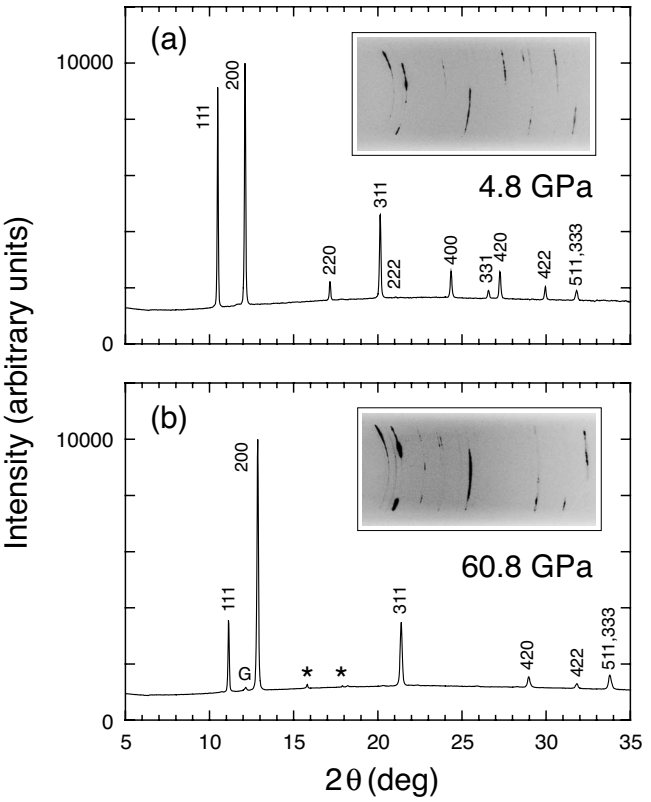

FIG. 2. Powder x-ray diffraction patterns of a gold foil (run 5) at high pressures. The insets show a part of the raw diffraction images recorded on an imaging plate. G indicates the diffraction peak of the Re gasket, and asterisks indicate the diffraction peaks of the solid He.

Figure 5 shows representative ruby luminescence spectra at high pressures in run 5. The R_1 and R_2 peaks remained well separated up to the highest pressure. Figure 6 shows the R_1 peak width and the R_1-R_2 separation as a function of pressure for the runs 5 and 7. We notice that the R_1 peak width remains small up to the maximum pressure, while the R_1-R_2 separation increases above about 30 GPa. The increase in the R_1-R_2 separation indicates the presence of uniaxial stress in the solid He-pressure medium.

The stress states in the gold sample are evaluated from the full width at half maximum (FWHM) of diffraction peaks and the Γ plots mentioned in Sec. II B. Figure 7 shows the FWHM normalized with the diffraction angle 2θ as a function of pressure. In the case of foil (run 5), the normalized width hardly changes with pressure, whereas the width

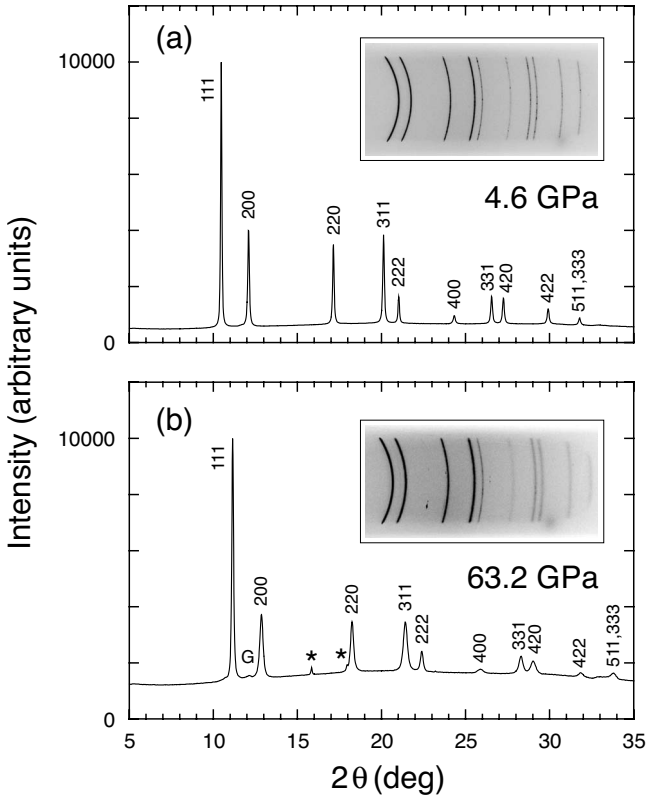

FIG. 3. Powder x-ray diffraction patterns of a gold powder (run 6) at high pressures. The insets show a part of the raw diffraction images recorded on an imaging plate. G indicates the diffraction peak of the Re gasket, and asterisks indicate the diffraction peaks of the solid He.

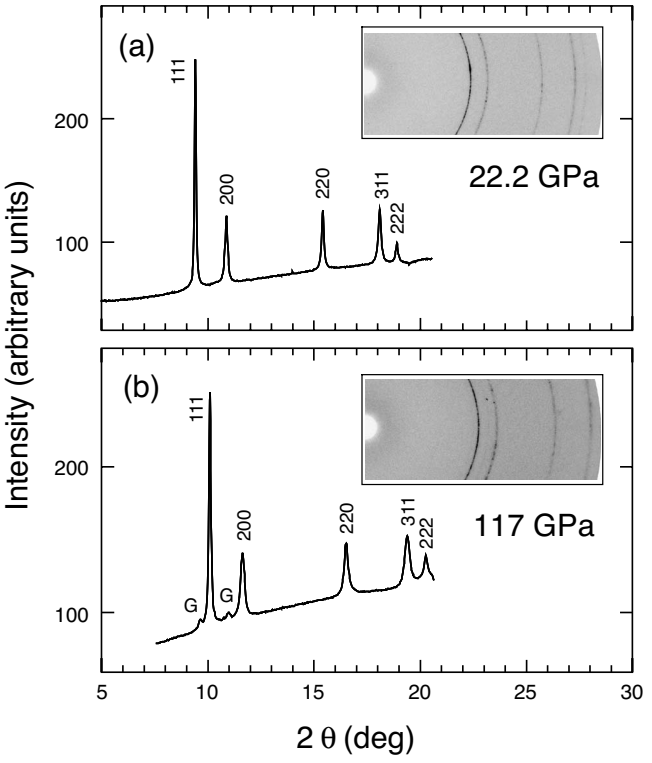

FIG. 4. Powder x-ray diffraction patterns of a gold powder grain (run 7) at high pressures. The insets show a part of the raw diffraction images recorded on an imaging plate. G indicates the diffraction peaks of the Re gasket.

steadily increases with pressure in the case of powder (runs 6 and 7). Since the powder forms an aggregate of fine grains, it is likely that microscopic stress develops between powder grains even if the aggregate itself is hydrostatically compressed. The 200 peak, for example, starts broadening from 5 GPa. The microscopic stress simply broadens the diffraction peaks and does not shift the peak positions from those expected for a single crystal hydrostatically compressed. There is no large peak broadening in the case of gold foil. The raw diffraction image (Fig. 2) indicates that the foil consists of large and oriented crystal grains. Because of the large crystal domains and relatively small number of grain boundaries, the foil may develop small microscopic stress under pressure.

Figure 8 shows typical Γ plots for runs 5–7. We notice that the slope of the Γ plots becomes positive in run 5 at high pressures, while it is negative in runs 6 and 7. As we will see in Sec. V, the positive (negative) slope gives negative (positive) uniaxial stress. Hence the stress state in run 5 is essentially different from runs 6 and 7. Table III summarizes the diffraction data of all our experimental runs.

V. DISCUSSION

A. Elastic parameters of gold under high pressure

In order to estimate the uniaxial stress component t from the Γ plots according to Eq. (6), we need the elastic anisotropy parameter S of gold under high pressure. No direct experimental estimate of this parameter is available for gold in the pressure range scanned here. Ultrasonic measurements of the elastic moduli of gold have been performed on single crystals in a limited pressure range.[2–5,37] Radial x-ray diffraction experiments have been performed up to 37 GPa.[38,39] Table IV summarizes the pressure derivatives dC_{ij}/dP from the literature. The elastic constants C_{ij} at higher pressures can be extrapolated from the values at atmospheric pressure C_{ij}^0 with the pressure derivatives dC_{ij}/dP by using the following formula:[42]

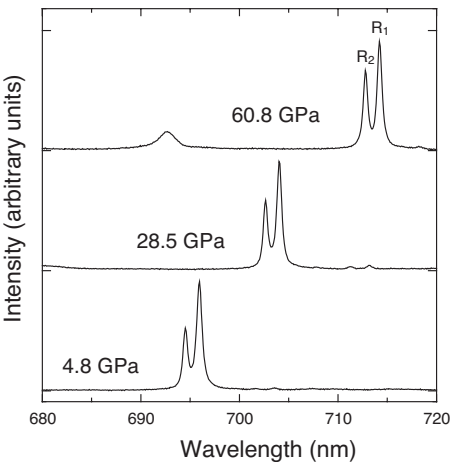

FIG. 5. Representative ruby luminescence spectra taken with a He-pressure medium in run 5.

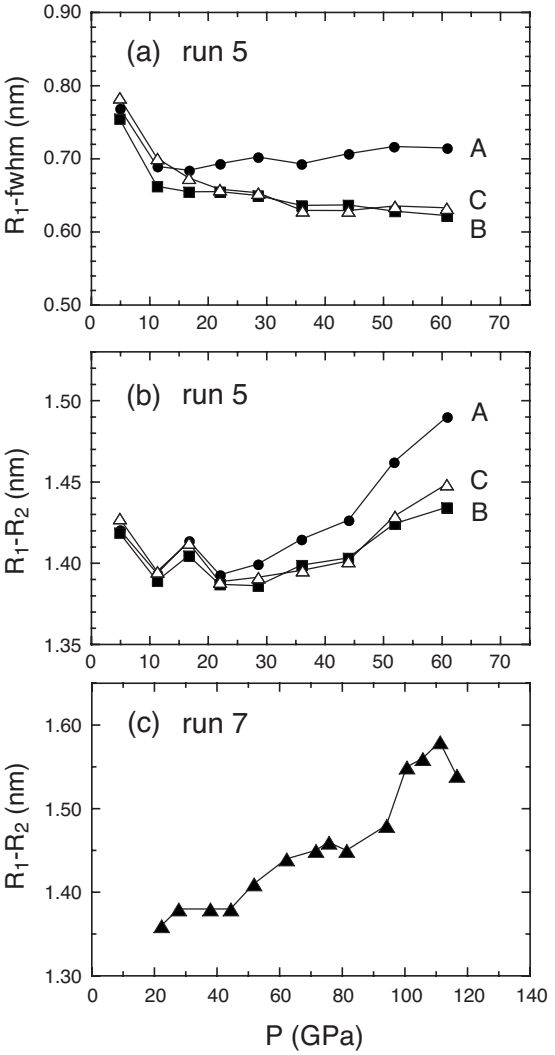

FIG. 6. Pressure dependence of (a) the peak width (FWHM) of the ruby R_1 luminescence line in run 5, (b) the R_1-R_2 separation in run 5, and (c) the R_1-R_2 separation in run 7. A, B, and C indicate the data of three ruby spheres in run 5 (see Fig. 1). The ruby A has larger peak width and R_1-R_2 separation under high pressure probably because it is caught by the gasket wall.

$$C_{ij} = C_{ij}^0 + (dC_{ij}/dP)P(V/V_0)^{1/3}, \tag{9}$$

where V/V_0 is expressed using the Murnaghan EOS. We use the following values for C_{ij}^0 at atmospheric pressure: C_{11}^0 =192.4 GPa, C_{12}^0=163.3 GPa, and C_{44}^0=41.8 GPa, which are the averaged ones listed in Ref. 38. The elastic anisotropy parameter S is then obtained with Eq. (5), which can be expressed by C_{ij} as

$$S = 1/(C_{11} - C_{12}) - 1/(2C_{44}). \tag{10}$$

Figure 9 shows the variation in S with pressure based on the pressure derivatives from the literature. The ultrasonic values are in good agreement with each other, while the estimate from the radial diffraction experiments is significantly different. The elastic moduli calculated by first principles[40,41] are larger than the experimental ones at low pressure, but they get closer to the ultrasonic values around 100 GPa. We thus use the extrapolation of the ultrasonic values in this paper, specifically those calculated from the pressure derivatives given in Ref. 4.

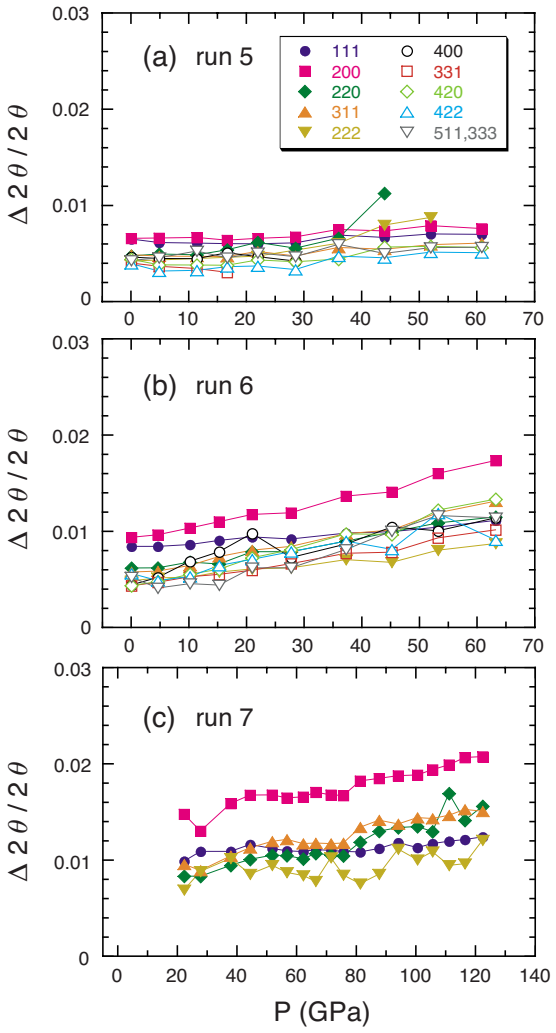

FIG. 7. (Color online) Variation in the width (FWHM) of x-ray diffraction peaks with pressure in (a) runs 5, (b) 6, and (c) 7. The peak width $\Delta 2\theta$ is normalized with the diffraction angle 2θ. The *hkl* indices are shown for each symbol in the inset of (a).

B. Stress states of gold

The uniaxial stress component t was calculated with Eq. (6) by assuming $\alpha \sim 1$, which gives the lower bound for t. The obtained values are listed in Table III and plotted in Fig. 10 as a function of pressure. The uniaxial stress component remains small up to about 30 GPa, above which it starts increasing. We note that the size of the x-ray beam, which is very different in our experiments, does not seem to affect the measured values of t. The t values are either positive or negative depending on the experimental runs. A negative uniaxial stress appears to be unusual because it means that the radial stress component σ_1 is larger than the axial stress component σ_3. We suppose that such a situation may be realized during the large deformation of the gasket hole under high pressure, which is typical for the He-pressure medium.

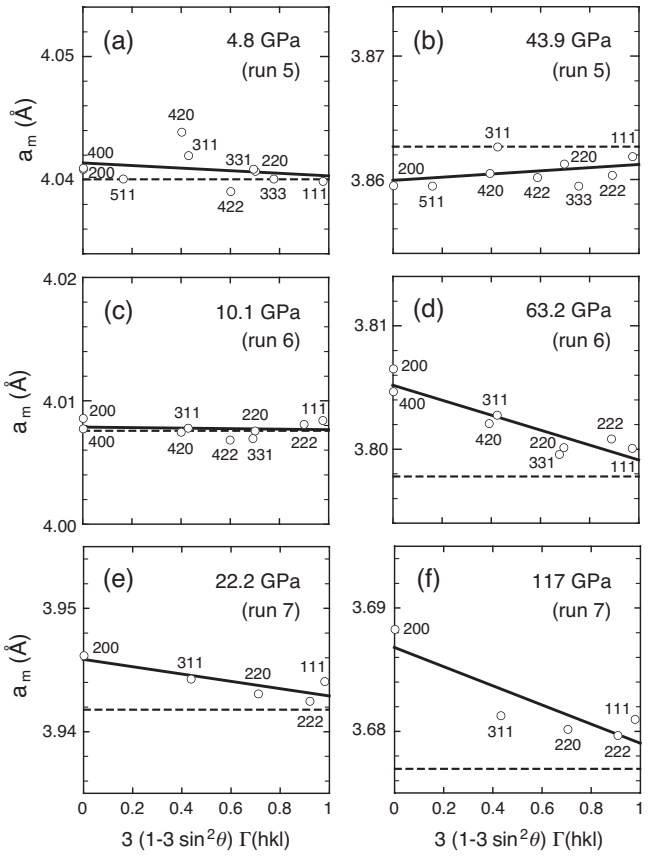

FIG. 8. Representative Γ plots for [(a) and (b)] run 5, [(c) and (d)] run 6, and [(e) and (f)] run 7. The dashed lines represent the lattice parameter under hydrostatic pressure a_p estimated with Eq. (11).

The negative uniaxial stress is observed for foil samples in runs 1 and 5.[43] The correlation between the negative uniaxial stress and the sample form is unclear. It should be noted that similar negative uniaxial stress was observed in the high-pressure experiments on Nb, where a lightly pressed powder was used as the specimen.[44] Further experimental study is necessary to investigate the mechanism of developing negative uniaxial stress. Radial x-ray diffraction technique should be useful for this purpose.[38,39]

Figure 11 shows a comparison of $a_m(111)$ and $a_m(200)$ obtained in runs 1 and 6. The lattice parameters determined from other reflections roughly fall in the range between $a_m(111)$ and $a_m(200)$. Run 1 exhibited negative uniaxial stress, while run 6 exhibited positive uniaxial stress. One notices that $a_m(200)$ deviates from $a_m(111)$ in opposite directions in the two runs. This is because the effects of uniaxial stress are reversed for negative and positive stresses [see Figs. 8(b) and 8(d)]. Consequently, if one takes an average of $a_m(hkl)$ for all hkl reflections and fits the $a_m(hkl)-P$ data, the fits systematically deviate for runs 1 and 6 as shown by the dashed and dash-dotted lines, respectively. This clearly demonstrates that the difference in stress states can be a reason for the deviation of the EOS parameters found in the literature.

In the present x-ray diffraction geometry, the lattice parameters obtained under positive uniaxial stress are larger than the hydrostatic values, while those under negative uniaxial stress are smaller.[15,22] The hypothetical hydrostatic data lie in between. A method is proposed to estimate the lattice parameter under hydrostatic pressure a_p from Eq. (1) by assuming $\alpha=1$ as given by the following equation:[30]

$$a_p = a_m(hkl)/\{1 + (t/3)(1 - 3\sin^2\theta)[S_{11} - S_{12} - 3S\Gamma(hkl)]\}. \quad (11)$$

The assumption $\alpha=1$ gives the smallest difference between a_p and $a_m(hkl)$. We have calculated a_p for each experimental run. Examples are shown by dashed lines in Fig. 8. Figure 12 shows the plot of $a_m(111)$, $a_m(200)$, and a_p in all runs around 50–70 GPa. The scatter of the data is much smaller for $a_m(111)$ than for $a_m(200)$. This is because $a_m(111)$ is least affected by the uniaxial stress, while the effect is largest for $a_m(200)$ in the case of gold (see Fig. 8). The scatter of a_p is comparable with that of $a_m(111)$. If a_p is correctly estimated by Eq. (11), it should show smaller scatter than $a_m(hkl)$, but this is not the case. We infer that the experimental errors in $a_m(hkl)$ and pressure exceed the small correction of $a_m(hkl)$ to a_p. In order to avoid the uncertainty in α in the estimation of a_p, we use $a_m(111)$ to determine the EOS parameters.

C. Isothermal EOS of gold

Figure 13 shows the plot of relative volume of gold as a function pressure, where the volumes are calculated from $a_m(111)$ and normalized to the value at atmospheric pressure ($V_0=67.847$ Å^3 and $a_0=4.0786$ Å in Ref. 34). The data are fitted to the Vinet form of EOS.[45] Since the bulk modulus of gold at atmospheric pressure is well established by ultrasonic measurements, we fixed B_0 to 167 GPa in the fitting procedure. We also fixed the relative volume at atmospheric pressure to 1. The fit of all the data yields $B_0'=5.51(1)$. It should be noted that a fit to the Birch-Murnaghan form of EOS (Ref. 46) yields a slightly smaller value of $B_0'=5.32(1)$. If we use the volumes calculated from a_p instead of $a_m(111)$, the fit to the Vinet EOS gives a value of $B_0'=5.43(1)$. Although the fitting error of B_0' is as small as 0.01 in each case, the actual error in B_0' should be larger[32] considering the uncertainty in S and α and the subsequent uncertainty in the effects of uniaxial stress on $a_m(111)$. The choice of different forms of EOS adds further uncertainty in B_0'. Hence we estimate the actual error in B_0' to be ~0.1 and propose that $B_0'=5.5(1)$ in the present work as far as when we use the ruby pressure scale by Zha *et al.*[14]

There are discussions that the current ruby scales underestimate pressure in the high-pressure range. A new ruby scale was proposed by Aleksandrov *et al.*[31] followed by various proposals by Holzapfel,[32] Dewaele *et al.*,[13] Chijioke *et al.*,[33] and Dorogokupets and Oganov.[18] In order to check the validity of the new ruby scales, the ruby pressures in the present experiments are converted with one of the new scales by Dorogokupets and Oganov (P' in Table III). The fit of the P'-$V_m(111)$ data to the Vinet EOS gives $B_0'=5.9(1)$, which is in excellent agreement with the ultrasonic values and theoretical calculations (Table I). The value of 5.88 for B_0' was

TABLE III. Lattice parameters $a_m(hkl)$ of gold under high pressure and the estimated uniaxial stress component t. We have assumed $\alpha=1$ in Eq. (6), which gives minimum values for t. Two pressure values P and P' are shown, which are based on the ruby scale given by Eq. (7) (Ref. 14) and Eq. (8) (Ref. 18), respectively.

			$a_m(hkl)$(Å)										
Run	P (GPa)	P' (GPa)	111	200	220	311	222	400	331	420	422	511, 333	t (GPa)
1	9.91	9.91	4.0083	4.0090	4.0076	4.0075	4.0073						0.04
	12.5	12.5	3.9927	3.9934	3.9901	3.9912	3.9906						0.07
	20.4	20.6	3.9508	3.9464	3.9496	3.9494	3.9501						−0.21
	27.2	27.6	3.9167	3.9130	3.9162	3.9153	3.9179						−0.25
	33.2	33.9	3.8916	3.8870	3.8916	3.8917	3.8943						−0.33
	40.1	41.1	3.8659	3.8636	3.8665	3.8662	3.8649						−0.12
	46.1	47.5	3.8474	3.8408	3.8484	3.8503	3.8448						−0.32
	52.9	54.8	3.8287	3.8204	3.8294	3.8287	3.8233						−0.45
	60.2	62.6	3.8053	3.7982	3.8028	3.8032	3.8022						−0.47
	65.9	68.8	3.7871	3.7830	3.7856	3.7853	3.7873						−0.37
	74.5	78.1	3.7632	3.7594	3.7615	3.7611							−0.34
	75.2	78.8	3.7629	3.7610	3.7601	3.7604							−0.15
	75.3	79.0	3.7632	3.7564	3.7610	3.7604							−0.61
2	2.27	2.25	4.0556	4.0612	4.0579	4.0605	4.0617	4.0584					
	3.43	3.41	4.0540	4.0538	4.0526	4.0539	4.0513	4.0496					−0.04
	4.99	4.96	4.0417	4.0424	4.0415	4.0413	4.0402	4.0400					0.00
	6.74	6.72	4.0352	4.0312	4.0308	4.0300	4.0301						−0.08
	7.84	7.82	4.0246	4.0240	4.0237	4.0231	4.0225	4.0220					−0.03
	9.24	9.23	4.0144	4.0154	4.0141	4.0141	4.0135						0.05
	10.6	10.6	4.0080	4.0078	4.0067	4.0068							0.00
	12.0	12.1	3.9990	4.0008	3.9980	3.9985	3.9969						0.12
	13.5	13.5	3.9905	3.9922	3.9898	3.9902	3.9889	3.9880					0.02
	15.0	15.1	3.9829	3.9848	3.9830	3.9826	3.9823	3.9814					0.02
	16.1	16.2	3.9770	3.9772	3.9762	3.9760	3.9751	3.9754					0.01
	17.4	17.5	3.9700	3.9712	3.9697	3.9693	3.9681	3.9709					0.09
	19.1	19.3	3.9617	3.9624	3.9609	3.9610	3.9591	3.9658					0.18
	20.8	21.0	3.9536	3.9538	3.9533	3.9528	3.9518	3.9529					0.03
	22.4	22.7	3.9460	3.9474	3.9457	3.9455	3.9442						0.11
	24.0	24.3	3.9383	3.9400	3.9386	3.9378	3.9373	3.9364					0.01
	26.2	26.6	3.9285	3.9302	3.9287	3.9282	3.9279						0.10
	27.9	28.4	3.9233	3.9238	3.9219	3.9226	3.9214						0.08
	30.1	30.6	3.9139	3.9142	3.9126	3.9116	3.9120	3.9099					−0.06
	1.14	1.13	4.0712	4.0708	4.0710	4.0712	4.0693	4.0680					−0.03
	0	0	4.0807	4.0804	4.0797	4.0791	4.0783	4.0780					−0.02
3	52.5	54.3	3.8314	3.8338	3.8311	3.8334	3.8330						0.15
	58.7	61.0	3.8136	3.8162	3.8136	3.8151	3.8150						0.17
	65.5	68.3	3.7952	3.7984	3.7960	3.7979	3.7956						0.28
	70.0	73.2	3.7817	3.7858	3.7827	3.7843	3.7828						0.33
	78.0	81.9	3.7625	3.7680	3.7632	3.7657	3.7634						0.49
	90.0	95.0	3.7338	3.7376	3.7330	3.7362	3.7346						0.38
4	31.0	31.6	3.9020	3.9060	3.9069	3.9073	3.9065						0.13
	36.2	37.0	3.8872	3.8914	3.8902	3.8904	3.8885						0.23
	39.5	40.5	3.8717	3.8780	3.8778	3.8778	3.8753						0.31
	45.3	46.7	3.8570	3.8566	3.8563	3.8562	3.8549						0.04
	50.2	51.9	3.8378	3.8406	3.8393	3.8403	3.8393						0.17

TABLE III. (*Continued.*)

			$a_m(hkl)$(Å)										
Run	P (GPa)	P' (GPa)	111	200	220	311	222	400	331	420	422	511, 333	t (GPa)
	55.3	57.3	3.8233	3.8248	3.8235	3.8241	3.8233						0.12
	66.5	69.4	3.7906	3.7924	3.7921	3.7922	3.7918						0.11
	74.1	77.6	3.7703	3.7732		3.7743	3.7724						0.22
	79.9	84.0	3.7583	3.7600	3.7590	3.7597	3.7586						0.16
	85.6	90.2	3.7459	3.7492	3.7463	3.7478	3.7464						0.31
5	4.81	4.78	4.0398	4.0408	4.0407	4.0420		4.0408	4.0407	4.0437	4.0392	4.0400	0.04
	11.4	11.4	3.9984	3.9998	4.0000	4.0012		3.9996	3.9984	4.0029	3.9976	3.9990	0.06
	16.6	16.7	3.9696	3.9716	3.9722	3.9740		3.9720	3.9683	3.9730	3.9692	3.9714	0.10
	21.9	22.2	3.9441	3.9446	3.9462	3.9488	3.9435	3.9472		3.9462	3.9510	3.9475	0.07
	28.5	29.0	3.9200	3.9148	3.9219	3.9196		3.9164		3.9180	3.9177	3.9153	−0.23
	36.0	36.8	3.8868	3.8840	3.8908	3.8868	3.8843			3.8863	3.8864	3.8826	−0.13
	43.9	45.2	3.8619	3.8596	3.8614	3.8625	3.8604			3.8603	3.8604	3.8597	−0.09
	51.9	53.7	3.8335	3.8326		3.8344	3.8365			3.8349	3.8330		−0.14
	60.8	63.2	3.8055	3.8060		3.8088				3.8098	3.8075		0.09
6	4.55	4.52	4.0453	4.0456	4.0444	4.0446	4.0450	4.0444	4.0438	4.0442	4.0436	4.0431	0.01
	10.1	10.1	4.0084	4.0086	4.0076	4.0078	4.0080	4.0076	4.0071	4.0075	4.0069	4.0057	0.01
	15.2	15.3	3.9791	3.9798	3.9785	3.9786	3.9785	3.9788	3.9779	3.9784	3.9790	3.9787	0.03
	20.9	21.1	3.9501	3.9512	3.9496	3.9498	3.9498	3.9520	3.9492	3.9493	3.9500	3.9470	0.09
	27.7	28.1	3.9210	3.9232	3.9208	3.9212	3.9203	3.9213	3.9196	3.9205	3.9216	3.9186	0.09
	37.2	38.1	3.8844	3.8888	3.8845	3.8865	3.8847	3.8869	3.8836	3.8850	3.8875	3.8865	0.24
	45.1	46.5	3.8559	3.8604	3.8560	3.8577	3.8561	3.8605	3.8552	3.8572	3.8586	3.8589	0.34
	53.2	55.1	3.8303	3.8366	3.8308	3.8331	3.8310	3.8343	3.8298	3.8318	3.8351	3.8368	0.40
	63.2	65.8	3.8001	3.8065	3.8002	3.8028	3.8009	3.8047	3.7996	3.8021	3.8042	3.8120	0.48
7	22.2	22.5	3.9441	3.9462	3.9431	3.9443	3.9425						0.15
	27.7	28.2	3.9181	3.9199	3.9180	3.9185	3.9175						0.11
	37.8	38.7	3.8796	3.8810	3.8785	3.8785	3.8797						0.07
	44.3	45.6	3.8566	3.8592	3.8555	3.8555	3.8579						0.11
	51.7	53.5	3.8317	3.8340	3.8305	3.8305	3.8323						0.13
	56.6	58.8	3.8164	3.8186	3.8148	3.8146	3.8144						0.21
	62.1	64.7	3.8007	3.8021	3.7985	3.7993	3.7989						0.17
	66.4	69.2	3.7880	3.7895	3.7860	3.7864	3.7855						0.20
	71.5	74.8	3.7748	3.7760	3.7721	3.7738	3.7709						0.27
	75.7	79.3	3.7644	3.7664	3.7623	3.7625	3.7614						0.28
	81.3	85.5	3.7513	3.7527	3.7488	3.7494	3.7467						0.31
	87.7	92.5	3.7364	3.7387	3.7339	3.7357	3.7312						0.47
	94.1	99.5	3.7222	3.7273	3.7214	3.7235	3.7222						0.53
	100.6	106.6	3.7107	3.7158	3.7098	3.7111	3.7076						0.68
	105.6	112.2	3.6999	3.7059	3.6989	3.7007	3.6959						0.86
	111.2	118.3	3.6902	3.6977	3.6876	3.6909	3.6906						0.84
	116.5	124.2	3.6810	3.6883	3.6802	3.6813	3.6797						0.89
	122.5	130.8	3.6699	3.6771	3.6677	3.6688	3.6740						0.58

obtained in Ref. 23. In that work, the effect of nonhydrostatic compression on gold EOS measured in Ref. 13 was corrected by a method different from the one chosen here. A very close value (5.9) was used by Dorogokupets and Dewaele[47] with the new ruby scale.[18] The value obtained here (5.9) should be considered as the definitive one since it is based on the largest data set (86 data points), which includes data published in Refs. 13 and 22 together with present data. Figure 14 shows the plot of B_0' as a function of B_0 from the present experiments and literature.

TABLE IV. Pressure derivatives of the elastic constants of gold. The derivatives are converted to dC_{ij}/dP if the original data are given by dC/dP, dC'/dP, and dB_s/dP, where $C=C_{44}$, $C'=(C_{11}-C_{12})/2$, and $B_s=(C_{11}+2C_{12})/3$. Ultrasonic (US) and radial x-ray diffraction (RXRD).

Ref.	Method	P_{max} (GPa)	dC_{11}/dP	dC_{12}/dP	dC_{44}/dP
Daniels and Smith (Ref. 2)	US	1	7.01	6.14	1.79
Hiki and Granato (Ref. 3)	US	0.006	5.72	4.96	1.52
Golding *et al.* (Ref. 4)	US	1	6.73	5.86	1.84
Biswas *et al.* (Ref. 5)	US	0.25	6.71	5.85	1.83
Song *et al.* (Ref. 37)	US	8	7.12	6.24	1.82
Duffy *et al.* (Ref. 38)	RXRD	37	6.03	4.3	0.9
Tsuchiya and Kawamura (Ref. 40)	Theory	100	5.97	5.38	1.43
Greeff and Graf (Ref. 41)	Theory	160	5.00	4.70	1.24

D. Gold as a pressure standard

In high-pressure experiments, the stress state of a sample is difficult to control with a solid-pressure medium. The stress state in the DAC is usually assumed to be simple with large axial and small radial stresses. This simple assumption was found to fail in the present experiments, which indicate the existence of negative uniaxial stress. The deformation of the gasket produces complex stress in the solids filled in the sample chamber. The variation in the stress states is a likely cause of errors in the pressure determination with a pressure standard. The lattice spacings of gold are easily affected by the uniaxial stress. If one ignores the uniaxial stress and simply takes an average of the lattice parameters determined from different d spacings, one gets volumes systematically biased and accordingly incorrect pressure values. In the case of gold, the lattice parameter determined from the 111 reflection can be used as the most reliable one since the effect of uniaxial stress is smallest for this reflection. The discrepancy of pressure values will then significantly decrease. The Γ plots are very useful to estimate the uniaxial stress in high-pressure diffraction experiments. We suggest including the magnitude of uniaxial stress as a part of data by which one can quantitatively evaluate the stress states of the high-pressure experiments.

Another point to be mentioned is the uncertainty in pressure determination with a solid-pressure medium. It is known that the pressure in a mixture of solids with different strength is different for each species.[48] This is directly relevant to the case, where a pressure standard and a specimen are compressed together with a solid-pressure medium.[49] Depending on the difference in the elastic moduli (bulk modulus, shear modulus, and the Poisson's ratio) of the pressure standard, specimen, and pressure medium, the pressure in each species

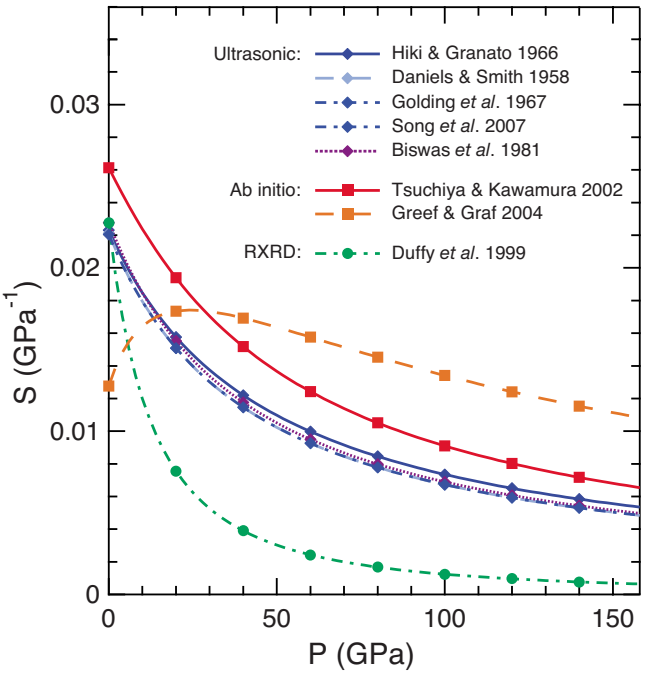

FIG. 9. (Color online) Evolution of the elastic anisotropy parameter S calculated from the pressure dependence of the elastic constants found in the literature (see Table IV for the references). The data by Golding *et al.* (Ref. 4) and by Song *et al.* (Ref. 37) are indistinguishable in this plot.

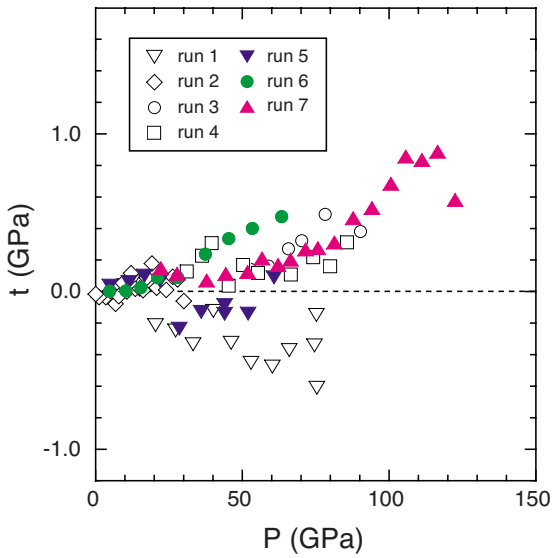

FIG. 10. (Color online) Uniaxial stress component t as a function of pressure. Open symbols show our previous data in runs 1–4, and closed symbols show the present data in runs 5–7. We have assumed $\alpha=1$ in Eq. (6), which gives minimum values for t.

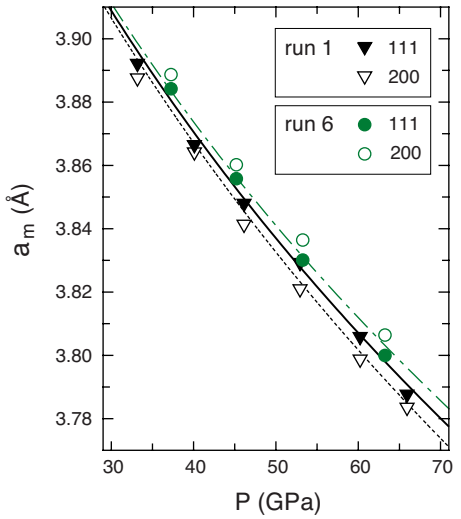

FIG. 11. (Color online) Lattice parameters $a_m(111)$ and $a_m(200)$ of gold as a function of pressure in runs 1 and 6. Other $a_m(hkl)$ falls in the range between $a_m(111)$ and $a_m(200)$. Notice that $a_m(200)$ in the two runs deviate in opposite directions relative to $a_m(111)$, corresponding to the negative and positive uniaxial stress components in each run. The dashed line shows a fit of the averaged data in run 1, and the dash-dotted line shows a fit of the averaged data in run 6. The thick solid line shows a fit to $a_m(111)$ with $B_0=167$ GPa and $B_0'=5.5$.

can differ by a factor of two in extreme cases.[48] This poses an essential problem in the pressure determination with a solid-pressure medium, but the problem disappears if a liquid pressure medium is used instead.

E. Hydrostaticity of the He-pressure medium

Helium is widely used as a hydrostatic pressure medium in modern DAC experiments. Takemura[22] reported that good

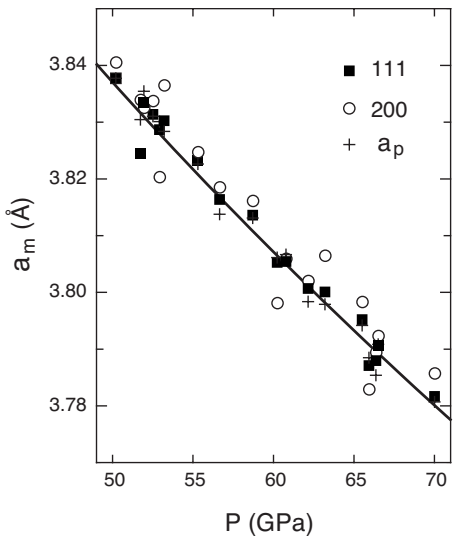

FIG. 12. Lattice parameter of gold as a function of pressure around 50–70 GPa. Closed squares are $a_m(111)$, and open circles are $a_m(200)$. Crosses show the lattice parameter under hydrostatic pressure a_p estimated with Eq. (11). The line shows a fit of $a_m(111)$ with $B_0=167$ GPa and $B_0'=5.5$.

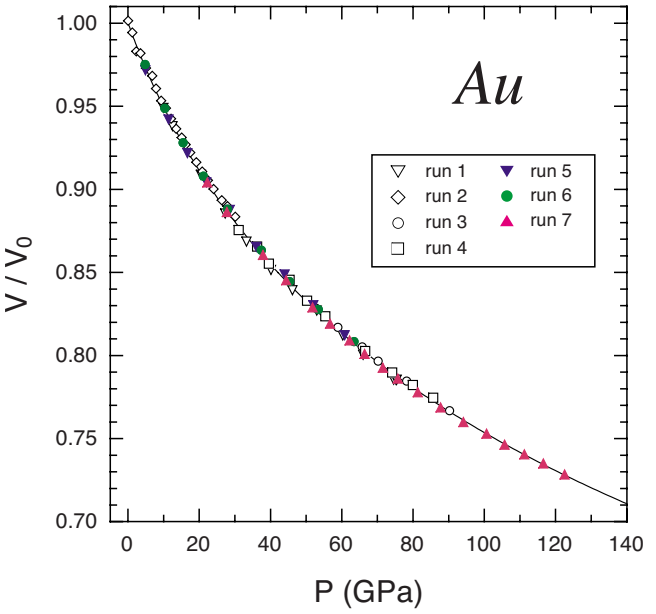

FIG. 13. (Color online) Pressure-volume relation of gold. Symbols distinguish each experimental run. The line shows a fit with $B_0=167$ GPa and $B_0'=5.5$.

hydrostatic conditions are maintained in solid helium to at least 50 GPa at room temperature based on the powder x-ray diffraction experiments on CeO_2, ZnO, and Au. The uniaxial stress in solid helium is considerably small compared with that in solid methanol-ethanol mixture. One should be careful, however, that the stress does exist in solid helium and affects the lattice spacings in some cases. The sensitivity to stress largely depends on the sample and properties to be measured. Aleksandrov *et al.*[31] studied a single crystal of diamond in a helium-pressure medium by x-ray diffraction

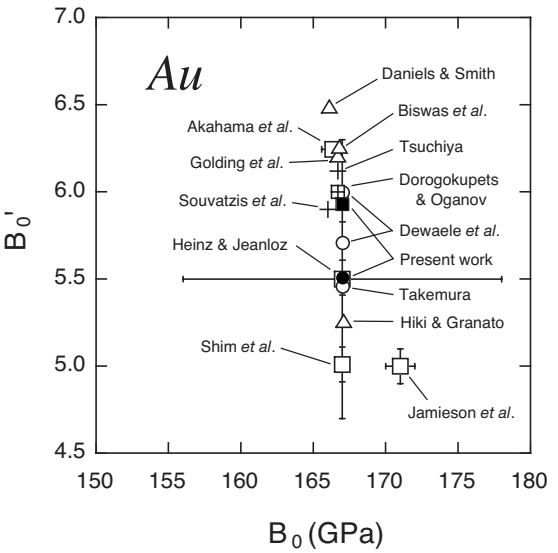

FIG. 14. Pressure derivative of the bulk modulus B_0' as a function of bulk modulus B_0 of gold. Open symbols show values found in the literature (see Table I for the references). The present results are shown by a closed circle for the current ruby scale (Ref. 14) and a closed square for the other ruby scale (Ref. 18).

and found that the rocking curve showed considerable broadening above about 35 GPa. The analysis of the EOS of metals compressed in solid helium shows that the effect of nonhydrostatic stress is negligible for Ag, Mo, and Cu up to 150 GPa, while it cannot be neglected in the case of Au.[23] The present results indicate non-negligible effects of uniaxial stress on the ruby luminescence spectra and gold diffraction data above about 30 GPa. The ruby R_1-R_2 separation increases above 30 GPa (Fig. 6), which is also noticed in the data shown in Ref. 22. The Γ plots of the original diffraction data[22] give uniaxial stress components, which start increasing above about 30 GPa (run 1 in Table III). There is no doubt that helium is an excellent pressure medium. On the other hand, the stress should not be neglected in the 100 GPa range at least for gold.

VI. SUMMARY

We have performed powder x-ray diffraction experiments on gold under high pressure with the He-pressure medium. The analysis of the diffraction data utilizing the Γ plots shows that the stress states of gold are close to hydrostatic up to the solidification pressure of helium at about 12 GPa. At higher pressures, nonhydrostatic stress gradually develops. The magnitude of the stress depends on the experimental conditions such as the sample form and the deformation of the gasket hole even if one uses the He-pressure medium. In some cases, we observed negative values of the uniaxial stress component. The measured lattice parameters $a_m(hkl)$ are biased by the uniaxial stress, which is a likely cause of the disagreement of the EOS parameters of gold found in the literature. The Γ plots indicate that $a_m(111)$ is least affected by the uniaxial stress in the case of gold. Actually, if we plot $a_m(111)$ as a function of pressure, it shows excellent agreement for all our experimental data. We have fitted the P-V data calculated from $a_m(111)$, fixing the bulk modulus at atmospheric pressure to $B_0=167$ GPa. The fit gives $B_0'=5.5(1)$ for the current ruby pressure scale[14] and 5.9(1) for the other ruby pressure scale.[18] Since the latter value is in excellent agreement with the ultrasonic values and theoretical calculations, the present experiments offer a support to the latter ruby scale. Finally, the analysis of the ruby luminescence wavelength R_1-R_2 separation and the uniaxial stress component of gold indicates that the stress state of the He-pressure medium gradually deviates from hydrostatic above about 30 GPa. This stress reaches non-negligible values in the pressure range above100 GPa at least for gold.

ACKNOWLEDGMENTS

K.T. acknowledges T. Kikegawa for the help in the synchrotron experiments. The experiments at the Photon Factory have been done under Proposal No. 2006G031. A.D. acknowledges the European Synchrotron Radiation Facility for provision of synchrotron radiation facilities on beamline ID27 and thanks P. Loubeyre and M. Mezouar for their interest and support.

*takemura.kenichi@nims.go.jp

[1] W. C. Overton, Jr., J. Chem. Phys. **37**, 116 (1962).
[2] W. B. Daniels and C. S. Smith, Phys. Rev. **111**, 713 (1958).
[3] Y. Hiki and A. V. Granato, Phys. Rev. **144**, 411 (1966).
[4] B. Golding, S. C. Moss, and B. L. Averbach, Phys. Rev. **158**, 637 (1967).
[5] S. N. Biswas, P. van't Klooster, and N. J. Trappeniers, Physica (Amsterdam) **103B**, 235 (1981).
[6] J. C. Jamieson, J. N. Fritz, and M. H. Manghnani, in *High Pressure Research in Geophysics*, edited by S. Akimoto and M. H. Manghnani (Academic, Tokyo, 1982), p. 27.
[7] H. K. Mao, P. M. Bell, J. W. Shaner, and D. J. Steinberg, J. Appl. Phys. **49**, 3276 (1978).
[8] D. L. Heinz and R. Jeanloz, J. Appl. Phys. **55**, 885 (1984).
[9] N. C. Holmes, J. A. Moriarty, G. R. Gathers, and W. J. Nellis, J. Appl. Phys. **66**, 2962 (1989).
[10] Y. Akahama, H. Kawamura, and A. K. Singh, J. Appl. Phys. **92**, 5892 (2002).
[11] H. K. Mao, J. Xu, and P. M. Bell, J. Geophys. Res. **91**, 4673 (1986).
[12] S.-H. Shim, T. S. Duffy, and K. Takemura, Earth Planet. Sci. Lett. **203**, 729 (2002).
[13] A. Dewaele, P. Loubeyre, and M. Mezouar, Phys. Rev. B **70**, 094112 (2004).
[14] C.-S. Zha, H.-K. Mao, and R. J. Hemley, Proc. Natl. Acad. Sci. U.S.A. **97**, 13494 (2000).
[15] K. Takemura, High Press. Res. **27**, 465 (2007).
[16] T. Tsuchiya, J. Geophys. Res. **108**, 2462 (2003).
[17] P. Souvatzis, A. Delin, and O. Eriksson, Phys. Rev. B **73**, 054110 (2006).
[18] P. I. Dorogokupets and A. R. Oganov, Phys. Rev. B **75**, 024115 (2007).
[19] T. Irifune, N. Nishiyama, K. Kuroda, T. Inoue, M. Isshiki, W. Utsumi, K. Funakoshi, S. Urakawa, T. Uchida, T. Katsura, and O. Ohtaka, Science **279**, 1698 (1998).
[20] S.-H. Shim, T. S. Duffy, and G. Shen, Nature (London) **411**, 571 (2001).
[21] L. Chudinovskikh and R. Boehler, Nature (London) **411**, 574 (2001).
[22] K. Takemura, J. Appl. Phys. **89**, 662 (2001).
[23] A. Dewaele and P. Loubeyre, High Press. Res. **27**, 419 (2007).
[24] J. M. Besson and J. P. Pinceaux, Science **206**, 1073 (1979).
[25] G. J. Piermarini, S. Block, and J. D. Barnett, J. Appl. Phys. **44**, 5377 (1973).
[26] P. M. Bell and H. K. Mao, Year Book - Carnegie Inst. Washington **80**, 404 (1981).
[27] M. Chai and J. M. Brown, Geophys. Res. Lett. **23**, 3539 (1996).
[28] We use the term "quasihydrostatic" to indicate a nonhydrostatic condition with a negligibly small uniaxial stress component. Since the definition is rather qualitative, we keep the usage minimum in this article.
[29] A. K. Singh, C. Balasingh, H.-K. Mao, R. J. Hemley, and J. Shu,

J. Appl. Phys. **83**, 7567 (1998).
[30] A. K. Singh and K. Takemura, J. Appl. Phys. **90**, 3269 (2001).
[31] I. V. Aleksandrov, A. F. Goncharov, A. N. Zisman, and S. M. Stishov, Zh. Eksp. Teor. Fiz. **93**, 680 (1987); [Sov. Phys. JETP **66**, 384 (1987)].
[32] W. B. Holzapfel, J. Appl. Phys. **93**, 1813 (2003).
[33] A. D. Chijioke, W. J. Nellis, A. Soldatov, and I. F. Silvera, J. Appl. Phys. **98**, 114905 (2005).
[34] J. Donohue, *The Structures of the Elements* (Wiley, New York, 1974), p. 224.
[35] K. Takemura, P. Ch. Sahu, Y. Kunii, and Y. Toma, Rev. Sci. Instrum. **72**, 3873 (2001).
[36] H. Fujihisa (unpublished).
[37] M. S. Song, A. Yoneda, and E. Ito, Chin. Sci. Bull. **52**, 1600 (2007).
[38] T. S. Duffy, G. Shen, D. L. Heinz, J. Shu, Y. Ma, H.-K. Mao, R. J. Hemley, and A. K. Singh, Phys. Rev. B **60**, 15063 (1999).
[39] T. S. Duffy, G. Shen, J. Shu, H.-K. Mao, R. J. Hemley, and A. K. Singh, J. Appl. Phys. **86**, 6729 (1999).
[40] T. Tsuchiya and K. Kawamura, J. Chem. Phys. **116**, 2121 (2002).
[41] C. W. Greeff and M. J. Graf, Phys. Rev. B **69**, 054107 (2004).
[42] M. Guinan and D. Steinberg, J. Phys. Chem. Solids **36**, 829 (1975).
[43] A small negative uniaxial stress was also observed in run 2 with a powder sample, but it is within the experimental error of t.
[44] T. Kenichi and A. K. Singh, Phys. Rev. B **73**, 224119 (2006).
[45] P. Vinet, J. Ferrante, J. H. Rose, and J. R. Smith, J. Geophys. Res. **92**, 9319 (1987).
[46] F. Birch, J. Geophys. Res. **83**, 1257 (1978).
[47] P. I. Dorogokupets and A. Dewaele, High Press. Res. **27**, 431 (2007).
[48] V. V. Avilov and R. G. Arkhipov, Solid State Commun. **48**, 933 (1983).
[49] I. V. Aleksandrov, A. F. Goncharov, I. N. Makarenko, and S. M. Stishov, Phys. Rev. B **43**, 6194 (1991).